Reprocessing the CROP95-M18 vintage multichannel seismic data acquired in the northern Adriatic Sea: the case of high penetration crustal profile recorded in shallow waters

G. Brancatelli, M. Busetti, M. Dal Cin and E. Forlin

National Institute of Oceanography and Applied Geophysics - OGS, Trieste, Italy

ABSTRACT   The CROP95-M18 seismic profile was acquired in 1995 as part of the *"CROsta Profonda"* project, a regional survey carried out to explore the deeper structures of the Earth's crust in Italy. Although the high energy of the source allowed a high penetration depth, the vintage stacked section showed some areas of low signal-to-noise ratio, due to the acquisition in shallow water environments and related reverberations of surface and guided-waves. To improve the quality of the image, we reprocessed the 2D seismic line with the up-to-date processing techniques by adopting a specific workflow in time domain up to pre-stack time migration. In addition, we created an accurate interval velocity model by combining the coherency inversion technique and reflection tomography. This resulted in depth migration of the uppermost part of the profile (to a depth of 9 km), which was confirmed by the stratigraphy of the Amanda 1bis well. The reprocessing significantly improved the image of the profile and enabled new information on the seismo-stratigraphy to be gleaned from the vintage data. This was particularly important for science and research, as new seismic data with high penetration depths, such as the CROP profiles, are currently difficult to acquire.

Key words: CROP, vintage seismic data, seismic processing, velocity modelling, depth imaging, northern Adriatic Sea.

1. Introduction

The transition to renewable energy and the environmental impacts associated with acquisition make new seismic data more difficult to obtain. This problem is particularly acute in the academic and public research worlds, especially in the field of Earth sciences. However, a large amount of seismic data has been collected over the past 50 years. Therefore, reprocessing old data with modern technologies is becoming increasingly important to enhance and renew the value of the data. Some examples of seismic reflection reprocessing of different data sets can be found in literature, e.g. Sopher and Juhlin (2013); Górszczyk *et al*. (2015); Nicholls *et al*. (2015); Munteanu *et al*. (2018); Civile *et al*. (2021); Brancatelli *et al*. (2022). In addition, some seismic lines of the CROP (*"CROsta Profonda"*, meaning "Deep Crust") data set were reprocessed, for example, by Mazzotti *et al*. (2000), Tognarelli *et al*. (2011), Busanello *et al*. (2017), and Berra *et al*. (2019). Depending on the type of data (both acquisition configuration and acquisition environment), specific processing sequences must be chosen. In this regard, the challenge is to adapt the up-to-date processing steps, such as deghosting, removal of multiples, and pre-stack time or depth migration, to the old data.

In this paper, we present the time reprocessing and depth imaging of the CROP95-M18 seismic line acquired in the northern Adriatic Sea. This line is part of the CROP project, an Italian joint cooperation between CNR (the Italian National Research Council), ENEL (the Italian National Electricity Authority) and ENI-AGIP (an Italian oil company), whose lines were acquired by OGS (*Osservatorio Geofisico Sperimentale*, nowadays OGS - National Institute of Oceanography and Applied Geophysics) in the 1980s and 1990s to explore the deep part of the crust, onshore and offshore of the Italian peninsula (Scrocca *et al.*, 2003; Finetti, 2005). The line was processed in 1997 by ENI-AGIP using what was, then, a standard sequence. This included predictive deconvolution, multiple attenuation by F-K filtering, velocity analysis, stack and post-stack filtering. The stacked section is affected by coherent noise (short- and long-period multiples) caused by the shallow water environment (water depth varies between 20 and 26 m along the line, Fig. 1), especially in the north-eastern part (below the top of the carbonate platform). Therefore, the objective of this study is to improve the signal-to-noise ratio of the seismic line compared to the old processed stacked section.

Marine seismic data acquired in very shallow water are usually highly contaminated by coherent noise (such as direct waves, surface waves, and guided waves). Some authors exploit these undesired coherent events in order to extract accurate near-surface P- and S-wave velocity models or physical properties (e.g. Kugler *et al.*, 2007; Boiero *et al.*, 2013; Wang *et al.*, 2016; Giustiniani *et al.*, 2020).
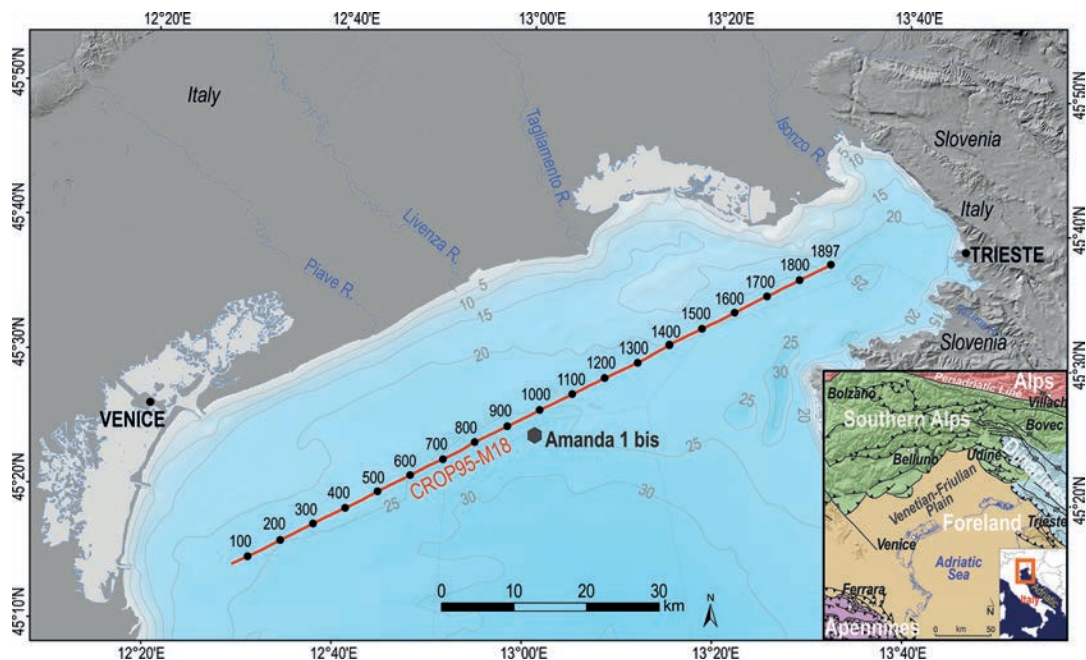

Fig. 1 - Location map of the CROP95-M18 profile acquired in the northern Adriatic Sea in 1995. The MCS profile CROP95-M18 is represented by the red line with position of every 100 shot points. Bathymetry is represented by a grid with cells of 50 m and by contours every 5 m, gridding performed by Zampa (2020), by using grids from EMODnet (2018) and Trobec *et al*. (2018). Digital Elevation Model compiled for Italy [5-m and 10-m cells by IDT-RV (2017) and IRDAT-FVG (2017), respectively], Slovenia [10-m cells; Arso (2017)] and Istria [25-m cells; EEA (2017)]. Map compiled shows the Alpine, Apenninic, Dinaric chains and relative foreland domain, together with the main tectonic structures [modified after Dal Cin *et al*. (2022), tectonic information from Ambrosetti *et al*. (1987); Galadini *et al*. (2005); Burrato *et al*. (2008); Zanferrari *et al*. (2008); Placer *et al*. (2010); Cucchi *et al*. (2013); Jurkovšek *et al*. (2016)]. Map compiled by using ArcGis® software from ESRI®; datum WGS84, projection UTM33.

In this study, we designed a specific processing flow to attenuate the noise (both coherent and incoherent) and increase the signal-to-noise ratio in the final seismic image. In addition, we adopted a broadband frequency approach to increase both the low and high frequency content of the seismic signal. Although the CROP95-M18 line was acquired to investigate the deep crust, we tried to improve investigation not only of the deeper part but also of the shallower part of the seismic section through an accurate processing flow in time domain with the up-to-date techniques. After noise reduction, we focused on seismic imaging firstly by creating a pre-stack time migration (PSTM) section through an iterative velocity analysis and, then, we moved to the depth domain to perform pre-stack depth migration (PSDM). Since depth imaging requires accurate velocity modelling, we used the coherency inversion technique (Landa *et al.*, 1988; Yilmaz, 2001) to obtain an initial velocity model that was refined by the layer-based reflection tomography. The velocity model was integrated and validated with velocity information extracted from the sonic log of the Amanda 1bis well (located in the central part of the CROP95-M18 profile, Figs. 1 and 2) and with the first-arrival traveltime tomography of the CROP95-M18 data.

The CROP95-M18 profile crosses the northern Adriatic Sea, located in the north-eastern corner of the Adria plate, and provides a unique image of the geological history of the area. The profile was interpreted by Finetti and Del Ben (2005), who distinguished the lower and upper crustal units and used the 7,290-m deep Amanda 1bis well (ViDEPI Project, 2009) to identify the sedimentary and magmatic sequences from the late Palaeozoic to the Quaternary. The CROP95-M18 profile and the Amanda 1bis well were also used to characterise the occurrences of the offshore deep brackish and salty aquifers of the northern Adriatic Sea (Giustiniani *et al.*, 2022).

The main geodynamic phases of the area consist of:
- the Early Jurassic rifting that separated the extensive late Palaeozoic and Triassic carbonate platform, in the Belluno basin to the west and from the shallow water environment to the east, where the Friuli-Dinaric Carbonate Platform (FDCP) developed during the Jurassic and Cretaceous and, locally, also during the Cenozoic (Cati *et al.*, 1987; Zanferrari *et al.*, 2013);
- the Cenozoic triple vergence flexure that resulted from the early Cenozoic SW-ward propagation of the External Dinarides;
- the deposition of the Eocene flysch above FDCP, in the eastern part of the area;
- the mid-late Cenozoic southward propagation of the eastern Southern Alps with the deposition of the Miocene marls;
- the late Cenozoic NE-ward shift of the Apennine foreland with the Plio-Quaternary sedimentary fill.

2. Data

Between 1988 and 1999, about 1,300 km of seismic lines were acquired onshore and 8,687 km were acquired offshore as part of the CROP project (Finetti *et al.*, 2005). Eight of these profiles were acquired in the Adriatic Sea. In 1995, OGS acquired the CROP95-M18 multichannel seismic profile (MCS) with the R/V OGS Explora in the northern Adriatic Sea (Fig. 1).

The acquisition of the whole line (97.3 km) was carried out with a 4,500-m long streamer of 180 channels spaced every 25 m (Table 1). A 50-m shot interval was selected, resulting in 4,500% fold coverage. In 1997, ENI-AGIP completed the processing of the line using a standard processing sequence up to a time stacked section (Finetti *et al.*, 2005; ViDEPI Project, 2009). The processing included resampling of data to 8 ms, reduction to 90 channels, trace equalisation,
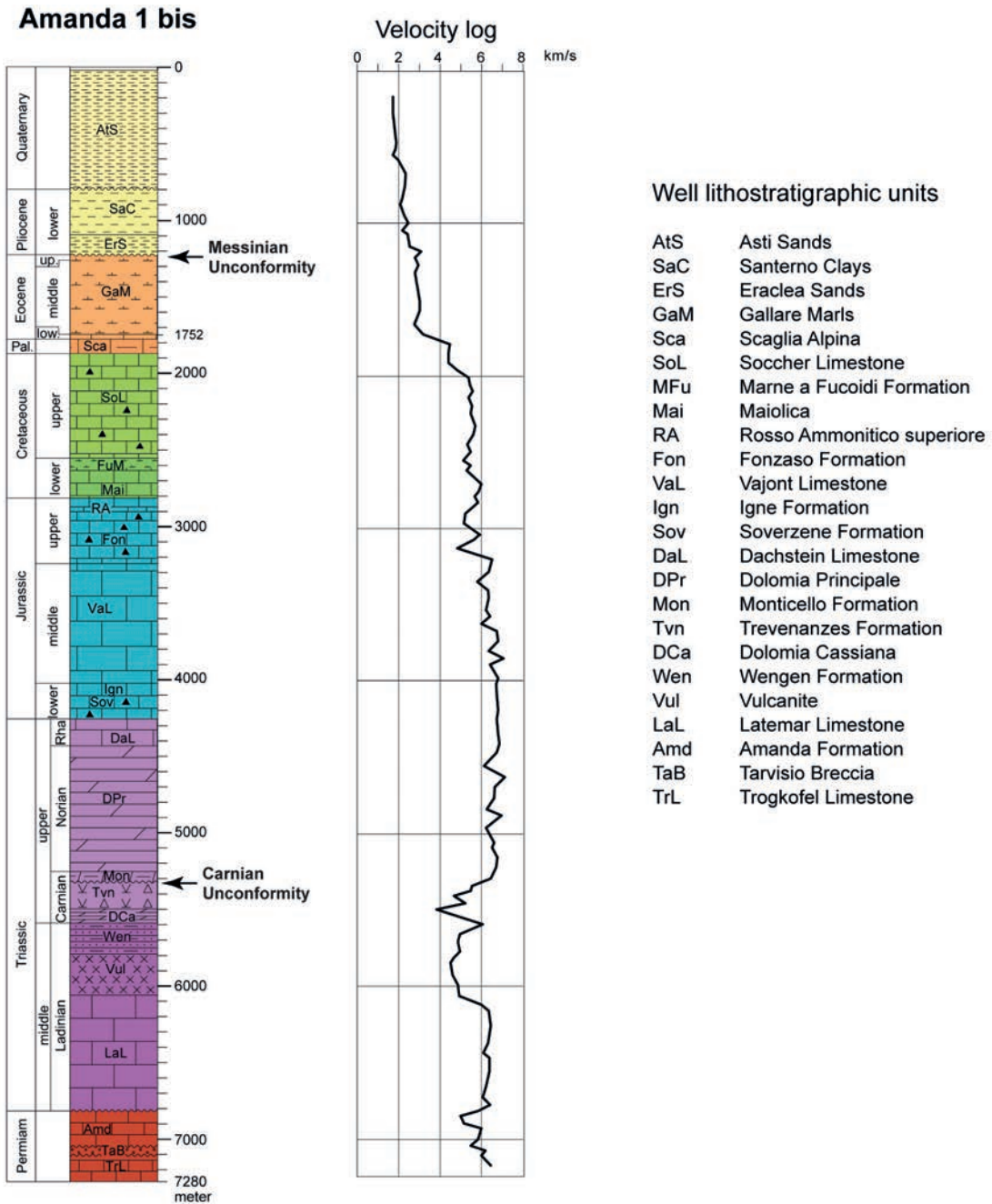
Well lithostratigraphic units

AtS	Asti Sands
SaC	Santerno Clays
ErS	Eraclea Sands
GaM	Gallare Marls
Sca	Scaglia Alpina
SoL	Soccher Limestone
MFu	Marne a Fucoidi Formation
Mai	Maiolica
RA	Rosso Ammonitico superiore
Fon	Fonzaso Formation
VaL	Vajont Limestone
Ign	Igne Formation
Sov	Soverzene Formation
DaL	Dachstein Limestone
DPr	Dolomia Principale
Mon	Monticello Formation
Tvn	Trevenanzes Formation
DCa	Dolomia Cassiana
Wen	Wengen Formation
Vul	Vulcanite
LaL	Latemar Limestone
Amd	Amanda Formation
TaB	Tarvisio Breccia
TrL	Trogkofel Limestone

Fig. 2 - Lithostratigraphy of the exploration well Amanda 1bis (modified after Nicolich *et al.*, 2004; ViDEPI Project, 2009) and velocity log (modified after Patricelli and Poli, 2020).

predictive deconvolution, multiple attenuation by F-K filtering, velocity analysis, application of normal moveout (NMO) and stacking, zero-phase conversion, post-stack F-K filtering, radial predictive filtering, and time variant filtering (TVF). This processing sequence resulted in a final section where the position of the image targets was not correct and the diffraction hyperbolas were not collapsed (Finetti *et al.*, 2005). This is clearly visible in some areas of the vintage

section, such as in the south-western part, between shot point (SP) 300 and 1,000 and between 3.5 and 6 s TWT (two-way traveltime; Figs. 9 and 11). Moreover, in the eastern part, the top of the FDCP surface-related multiples affect the deeper seismic data and the reflection of the Carnian unconformity is discontinuous and not so evident. Finally, the reduction to 90 channels (by summing two adjacent traces within a shot gather) improved the signal-to-noise ratio at the cost of lowering the lateral resolution.

Table 1 - Acquisition parameters for the CROP95-M18 profile, acquired in 1995.

Source	32 airgun array, 80.4 l volume
Source depth	8 m
Streamer length	4,500 m
Streamer depth	12 m
Number of channels	180
Number of hydrophones/group	32
Shot interval	50 m
Near offset	150 m
Sample rate	4 ms
Record length	17 s (TWT)
Recording filters	Low cut out; High cut 77 Hz 70 dB/oct

The Amanda 1bis well, located 2,250 m SE of the CROP95-M18 seismic line, was drilled offshore in 1979 by a joint venture of the oil companies ENI-AGIP, INA Naftapline, SIR, and ELF and reached a depth of 7,305 m below sea level (b.s.l.) (ViDEPI Project, 2009). The perpendicular line intercepts the CROP95-M18 line at approximately SP 940.

The Amanda 1bis well recovered the Permo-Triassic carbonates, vulcanites, and terrigenous sediment topped by the Carnian unconformity, a regional erosional event, which is usually well-imaged in seismic profiles. Above the Carnian unconformity, Meso-Cenozoic carbonates, approximately 3.5 km thick, were deposited from the shallow Triassic platform to the Jurassic-Paleocene deep-water basinal environment. With the ending of the carbonate sedimentation, the Gallare marls (middle Eocene to Miocene) filled the basin. They were topped by the Messinian unconformity, a regional erosional marker related to the sea level drop caused by the Messinian Salinity Crisis in the Mediterranean Sea that caused extensive erosion in the subaerial environment (Fantoni *et al*., 2002). Plio-Quaternary sediment covers the Gallare marls (Fig. 2).

In the north-easternmost Adriatic Sea, multichannel seismic investigation provides evidence of the FDCP, which developed during the Cretaceous, and was overlain by the terrigenous sediments of the Eocene flysch during the Dinaric compression phase (Busetti *et al*., 2010). During the late Oligocene - Middle Miocene, the terrigenous-carbonate sediment of the Cavanella Group draped over the Mesozoic FDCP margin and the Gallare marls (Zecchin *et al*., 2022), representing the beginning of the Alpine compression phase.

ENI also acquired the velocity log in the Amanda 1bis well [presented in Patricelli and Poli (2020)], while we have no information on the density characteristics of the drilled formations.

3. Methods

To analyse the CROP line, we performed three main steps: 1) reprocessing of data through a modern processing sequence in time domain up to a PSTM section (Fig. 3); 2) velocity modelling and depth migration; 3) validation of the interval velocity field and depth migrated section. The latter result was achieved using first arrival traveltime tomography and information obtained from the Amanda 1bis well (i.e. sonic log and formation top).
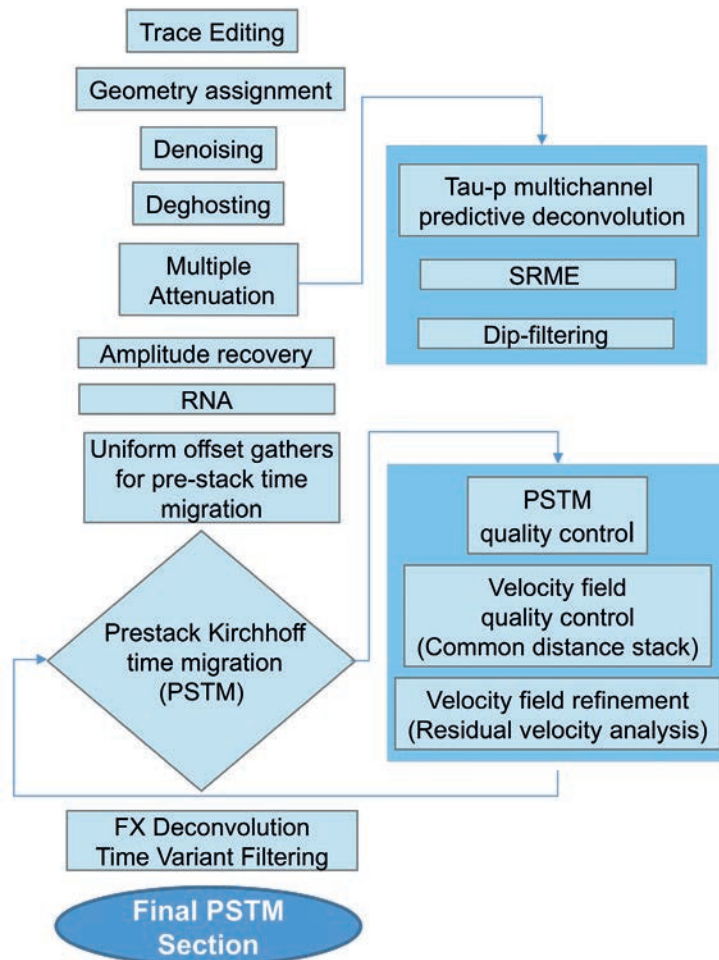

Fig. 3 - The adopted processing flow in time domain for the CROP95-M18 line.

Starting with time domain reprocessing, the denoise step aimed to remove all the incoherent (random) noise (i.e. amplitude bursts and spikes) and the coherent noise, represented by non-reflection events such as direct waves, refracted waves (diving and head waves), guided and Scholte (1942, 1947) waves (Fig. 4).

Direct and refracted waves significantly affect the first part of the recorded data (reflections from the water bottom and shallow sediments). As a matter of fact, considering the very shallow water depth (between 20 and 26 m b.s.l.) and the acquisition geometry (offsets and both source
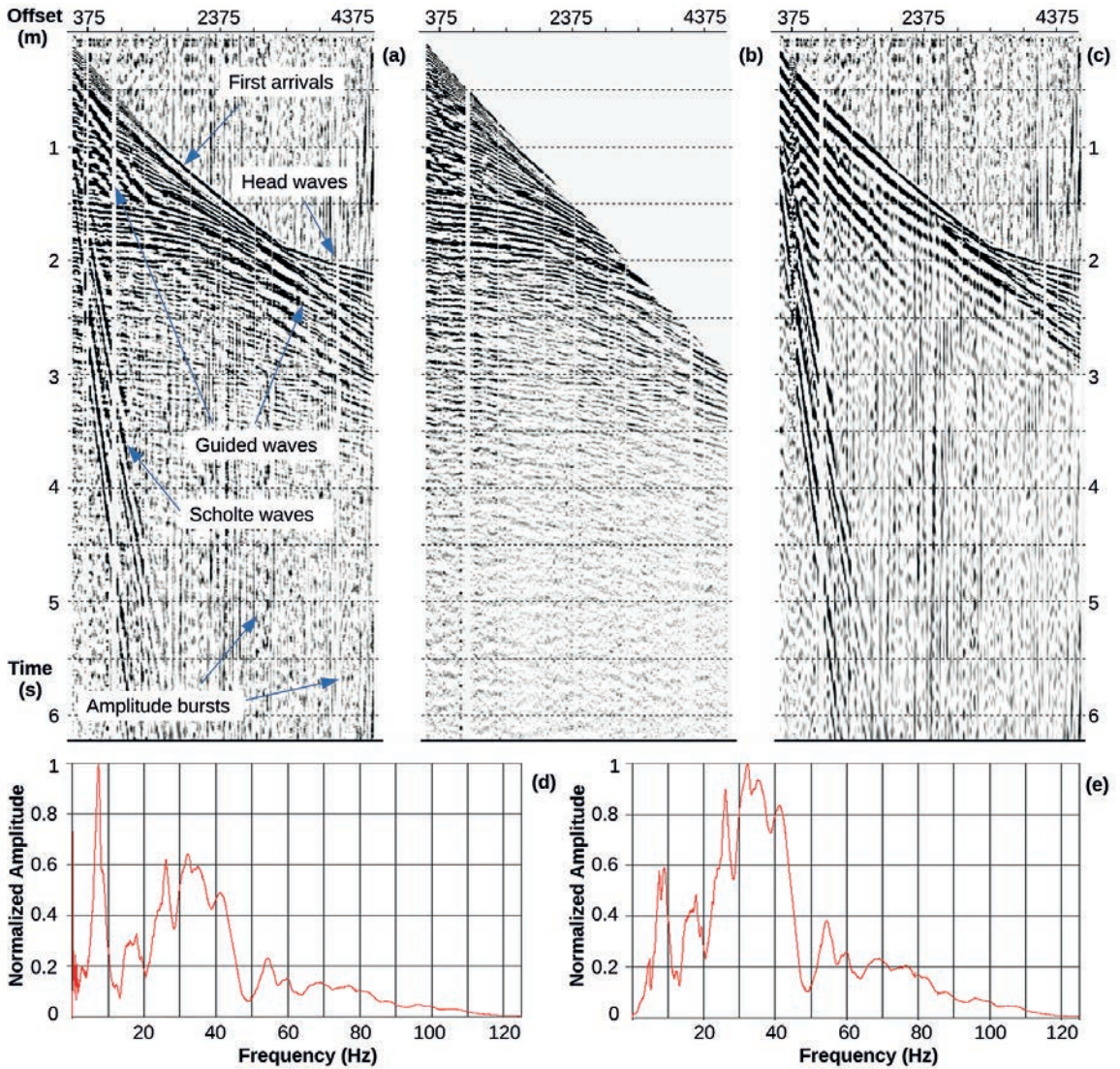
Fig. 4 - An example of raw shot gather (a) with its frequency spectrum (d). The same shot gather after the denoise step (b) with its frequency spectrum (e). The difference between raw and processed shot gathers (c).

and receiver depths), it is possible to calculate the arrival time of the direct wave, which almost coincides with that of the water bottom reflection for all the offsets of the shot gathers (the maximum deviation is 2 ms). Furthermore, considering a velocity range between 1,600 and 1,900 m/s for the first sediments below the water bottom, and referring to Snell's law and the simple geometry concerning refraction waves, it can also be concluded that the critical distance (about 91 m for a sediment velocity of 1,600 m/s or 40 m for a sediment velocity of 1,900 m/s) is lower than the near offset (150 m). Scholte waves are interface waves that occur along a solid-fluid boundary and propagate along the seafloor at low velocity, low frequency and high amplitude (Rauch, 1986). Post-critical multiple reflections trapped into the water layers result in dispersive waves called guided waves (Burg *et al.*, 1951; Liner, 2012). Stacking usually attenuates guided waves but, in some cases (especially in the shallow parts where useful offsets are limited), they

may still be present and cause degradation of the stack image (Dondurur, 2018). Moreover, if guided waves and Scholte waves are not attenuated before stacking, they can adversely affect some processing steps, such as deghosting and deconvolution.

Therefore, we first muted data for a shorter time than that of the arrival of the first water bottom reflection. Guided waves are visible on the shot gathers of CROP95-M18 at early arrivals as parallel lines, just below the first arrival refracted events (Fig. 4a). Since these are linear coherent events, we isolated them by using the radial trace transform (Henley, 1999). This tool extracts the amplitudes along straight lines by mapping data from the *x-t* (offset-time) domain to the *v-t'* (apparent velocity-time) radial domain. Then, the guided waves were transformed back to the offset-time domain and adaptively subtracted from the original data (Fig. 4b). To avoid the loss of primary signals at high frequencies (particularly important in the shallower part of the data), the radial forward and inverse trace transformation was applied only to frequencies below 20 Hz.

Scholte waves (Fig. 4a) are characterised by a narrow band spectral frequency (1-5 Hz in our data, Fig. 4d). Therefore, we used a band-limited noise reduction device, which decomposes the data traces into signal and noise components. The seismic traces were filtered in the 1-5 Hz range (by a bandpass Butterworth filter), and the result (noise component) was subtracted from the input traces (given the signal component). The envelopes of both components were evaluated and compared along time windows, and only where the noise envelope exceeded the signal envelope, it was scaled down to match the signal envelope (Robinson and Treitel, 1980; Oppenheim and Schafer, 1989). Finally, the signal and scaled noise components were summed to obtain the final trace. We also removed noise bursts by comparing the amplitudes of one trace with those of neighbouring traces of shot gathers. The comparison of amplitudes was done in overlapping time windows of 200 ms, and the anomalous amplitudes were scaled down. Once the denoise step was completed, it was possible to note that undesired events were attenuated and that, as a result, reflections appeared clearer and showed higher continuity, even in areas where they were not visible before (Fig. 4b). The difference between the original and processed shot gather demonstrated that noise alone was attenuated and the primary signals were preserved (Fig. 4c). Furthermore, the frequency spectrum proved more balanced because the low frequency (1-5 Hz) noise had been attenuated while the 10-45 Hz frequency band had been enhanced (Fig. 4e).

After denoising, we applied a deghost algorithm in the frequency domain, which recovered the ghost-free wavefield according to the minimum energy criteria (Yilmaz and Baysal, 2015), so as to increase the frequency bandwidth and enhance the low frequencies. The complete mathematical formulation can be found in Perz and Masoomzadeh (2014) or Yilmaz and Baysal (2015). In this paper, we simply recall that the ghost operator in the frequency-wavenumber domain can be expressed as $g(\omega) = 1 + \alpha e^{j\omega\tau}$, where ω is the angular frequency, α is the sea surface reflectivity, and τ is the ghost time delay, which, for normal incidence, is equal to $\frac{2d}{v}$ where d is the streamer (receiver ghost) or source (source ghost) depth and v is the water seismic velocity. Therefore, for a given source and receiver depth and seismic water velocity, it is possible to develop an inverse filter in the frequency domain to recover the ghost-free wavefield for all frequencies. During CROP95-M18 data acquisition, the streamer was towed at a mean depth of 12 m, while the mean depth of the airgun source was 8 m b.s.l. The deghost section shows an enhancement of the lower frequencies (about 5-12 Hz), which is evident in the deeper reflections (Figs. 5a and 5b) as well as in the frequency spectrum (Figs. 5c and 5d). The broadening of the frequency range is also significant at high frequencies (above 45 Hz).

One of the main challenges in a shallow water environment is the attenuation of multiples and short-period reverberations, which can severely degrade the seismic image. In such an
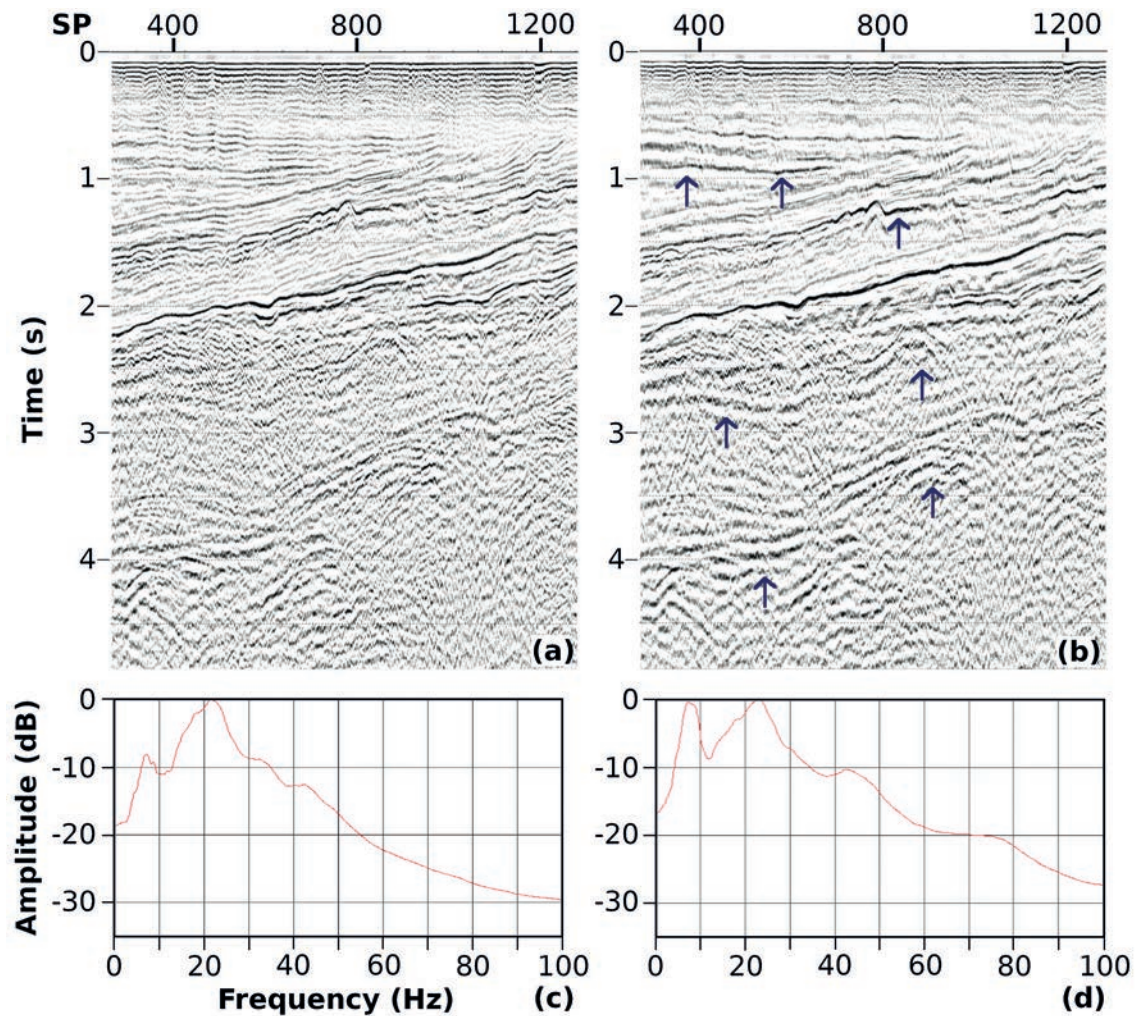
Fig. 5 - Portion of stacked section before (a) and after the application of deghost (b) with the corresponding frequency spectrum (c) and (d). The blue arrows highlight reflectors where it is possible to note the improvements due to the deghost step.

environment (very shallow water layer), the state-of-the-art of the multiples removal technique, and surface-related multiple elimination [SRME; Verschuur (1992)], cannot provide satisfactory results. In fact, the water bottom reflection is not recorded due to the near offset gap, while the post-critical reflections at small offsets do not contribute to the prediction of multiples (Hung *et al.*, 2010; Verschuur, 2013). On the other hand, predictive deconvolution in shallow and flat seafloor waters is usually very effective in attenuating short-period multiples. Hence, it is possible to adopt a strategy, which combines predictive deconvolution with SRME as suggested by Verschuur (2013). SRME is applied after predictive deconvolution to remove only the mid- to long-period multiples related to deep horizons. To optimise the results, we tested multichannel predictive deconvolution in both the time domain (Peacock and Treitel, 1969; Taner *et al.*, 1995) and the tau-*p* domain (Taner, 1980; Treitel *et al.*, 1982; Lokshtanov, 1995, 1999). Multichannel deconvolution in the tau-*p* domain has two main advantages. First, in the tau-*p* domain multiples become periodic for each reflection angle (*p*-parameter), whereas in the time domain this occurs

only for the zero offset. Moreover, by considering a multi-channel deconvolution process, it is possible to overcome the limitation arising from the assumption that the medium is supposed to be laterally invariant, which is at the base of the single-channel deconvolution (Verschuur, 2013). Looking at the results, the predictive deconvolution in time domain (Fig. 6b) can be seen to slightly attenuate the strong reverberations, while these are largely suppressed in the tau-*p* domain (Fig. 6c). In particular, it is clear that the ringing effect is almost completely attenuated with the tau-*p* deconvolution and that the section shows a sharper definition of the main reflectors. Furthermore, if we look at the autocorrelation functions, we can see that most of the energy is concentrated in the second zero crossing of the autocorrelation function and that reverberations (which appear as straight lines) are largely attenuated.
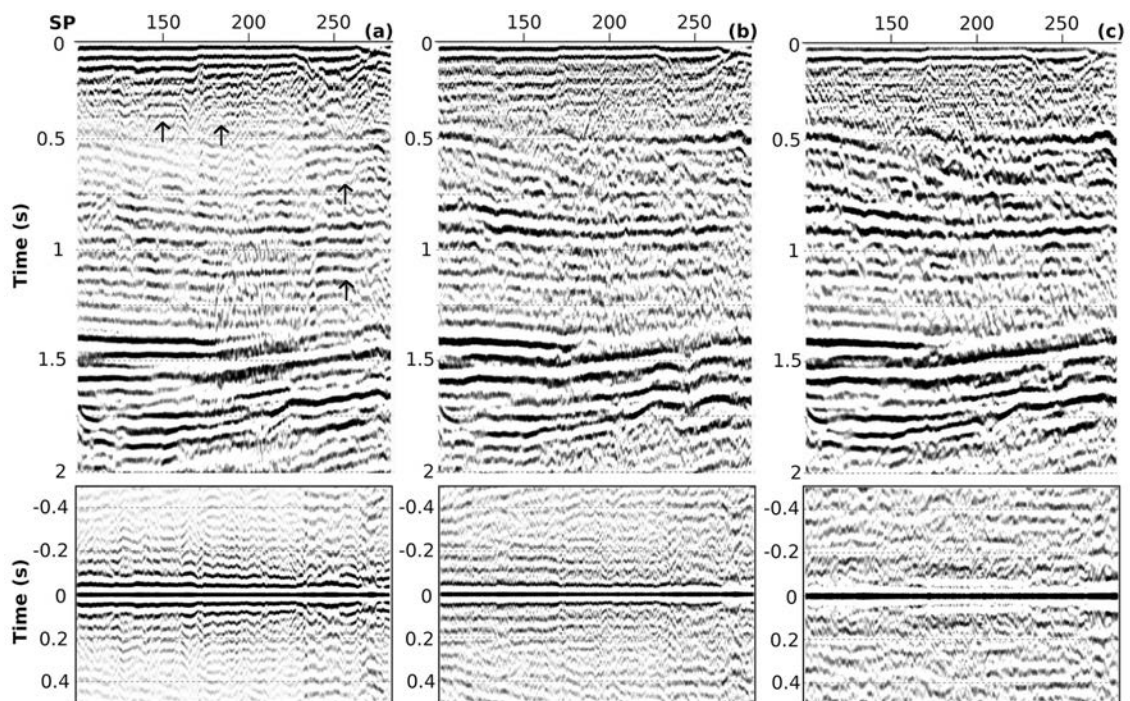

Fig. 6 - Portion of stacked section (top), with its relative auto-correlation (bottom), before (a) and after the application of multichannel predictive deconvolution, applied respectively in time (b) and tau-*p* domain (c). The black arrows depict some areas affected by strong reverberations.

In the eastern part of the section (nearby SP 1600), the top of the FDCP rises to about 250 ms TWT. This reflector and the overlying reflector (Plio-Quaternary unconformity) have high amplitudes that produce long-period surface-related multiples (such as the first "m1" and the second "m2" order multiples of the FDCP top, Fig. 7a), which were not removed by predictive deconvolution. For these reasons, we muted the water bottom reflections and shallow reflections up to 200-250 ms TWT, and only the remaining part of the seismic traces were used to predict these multiples with the SRME technique (Fig. 7c). Subsequently, the modelled multiples were adaptively subtracted from the original data by using a least-squares matching filter (Abma *et al.*, 2005), 60 ms long in rectangular windows of 11 traces x 500 ms. In this way, the multiples were strongly attenuated into the carbonate layer (Fig. 7b). To further attenuate the steep parts of the
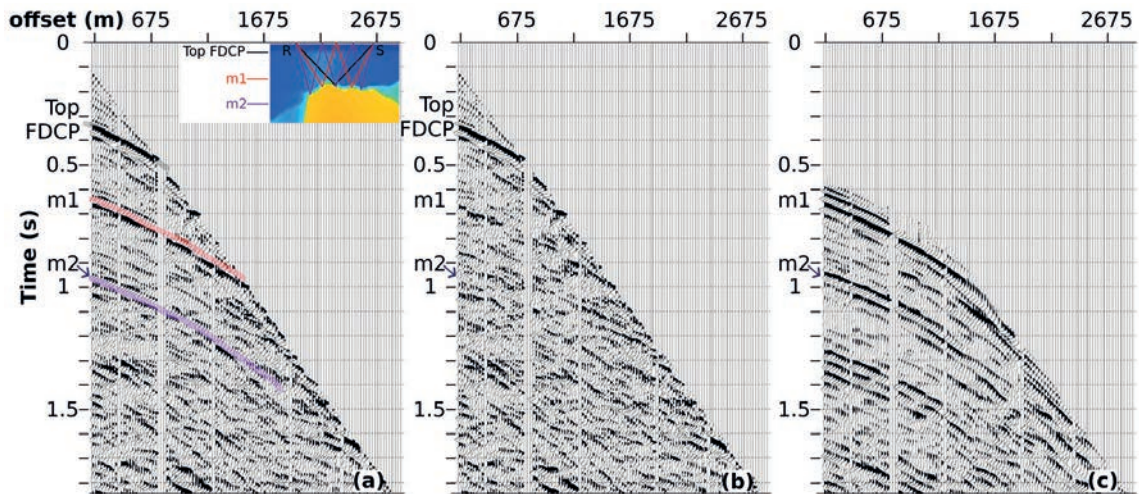
Fig. 7 - A shot gather before (a) and after (b) the adaptive subtraction of the modelled multiples, predicted by the SRME technique (c). Top FDCP indicates the primary reflection of the top of the Friuli-Dinaric Carbonate Platform, while m1 and m2 indicate respectively its first and second-order surface-related multiple. The inset at the top right of panel a represents a simple sketch of a ray path associated with the primary and its first and second order multiple reflection of the top FDCP layer.

residual multiples, we applied dip-filtering to the NMO corrected gathers, but only in a limited part of the section (in the eastern part, between SP 1,500 and 1,600). This type of filter, based on move-out discrimination between primaries and multiples, was applied in the F-K domain.

After attenuating the coherent noise, the amplitudes were recovered using the spherical divergence correction, and the signal-to-noise ratio was further increased by applying the random noise attenuation algorithm. We, then, applied a Kirchhoff PSTM algorithm to migrate the CROP95-M18 line. A recursive velocity analysis was performed on pre-stack migrated gathers until satisfactory quality control (both on the gathers and on the section) was achieved. To mitigate migration noise, we regularised the offsets within each common mid-point (CMP) gather by applying differential NMOs and correcting each trace for the difference between its original and the uniform offset. In this way we obtained CMP gathers of 45 traces, with a constant offset range between 150 and 4,550 m. As a final step, to further improve the quality of the PSTM section, a predictive Fx-deconvolution was applied, followed by TVF.

In a complex geological setting, depth imaging (achieved through depth migration) is required to define the real geometry and depth of the buried structures (Yilmaz, 2001). In addition, velocity modelling plays a crucial role in obtaining the best seismic image (Jones, 2018).

We combined the coherency inversion technique (Landa, 1988; Yilmaz, 2001) and reflection tomography (Jones, 2010) to build an interval velocity model in a layer-stripping way.

Coherency inversion is a method for estimating layer velocities based on ray theory and, in particular, on the inversion of seismic travel times (Landa *et al.*, 1988; Yilmaz, 2001). This method involves the construction of a subsurface layer model in the time domain, followed by ray-tracing to estimate the associated velocities. Starting from a trial velocity, a time-to-depth conversion of the chosen time horizon is calculated taking into account ray tracing at normal incidence. In this way, the layer base is obtained and a CMP ray-tracing, that models the travel time for the entire offset of a CMP gather, can be performed. Along this modelled trajectory, the coherency semblance spectrum is evaluated for the assumed trial velocity (Yilmaz, 2001). By repeating this

procedure for a range of possible velocities, the velocity that gives the highest semblance value at all CMP positions, where coherence inversion was performed, can be assigned to the layer. The velocity-depth model is built up layer-by-layer, from the shallowest to the deepest interpreted horizons. The great advantage of using coherency inversion to obtain a starting velocity model is that this technique respects ray bending at layer boundaries, by taking into account non-hyperbolic CMP travel times. This leads to a more realistic velocity model compared to a simple Dix's velocity conversion of the root mean square (RMS) velocities.

The coherency inversion was performed along five horizons: the seabed, the top of the Pliocene SW-ward progradations, the Messinian-Pleistocene unconformity (at the top of the Eocene-Miocene Gallare marls to the west and central profile belonging to the Messinian age, and at the top of the Cavanella Group and Eocene flysch in the easternmost part of younger age), the top of the Meso-Cenozoic carbonate sequences composed of the Scaglia (also known as Scaglia Alpina) to the west and the FDCP to the east, the Carnian unconformity (between the lower terrigenous and volcanic deposition and the upper Dolomia Principale). These horizons were also selected based on the stratigraphy and geophysical logs of the Amanda 1bis well (Patricelli and Poli, 2020), as they represent the chief velocity discontinuities that generate the main acoustic impedance contrasts visible in the seismic section. The horizons were picked on the PSTM section and, then, de-migrated (e.g. Brancatelli *et al.*, 2022). The water layer thickness was kept constant at a depth of about 20-25 m with a velocity of 1,520 m/s. Starting from the shallower horizon below the seabed, each layer depth and velocity were, therefore, first determined with coherency inversion and, then, refined with several layer-based tomography iterations, until a low residual error on common image gathers (CIG) was achieved. To check the consistency of our velocity-depth model, we analysed the CIGs and performed residual move out (RMO) analysis along the horizons (every 160 CIGs). The RMOs represent the input errors in the tomography, which updates both the velocity and depth of the interpreted layers at each stage. With the updated velocity field, we re-migrated our data and, then, iteratively repeated the layer-based tomography to minimise the errors. In the initial phase of our update loop, the RMOs on the CIGs were generally high, with areas that showed problems of undercorrection (too high velocity) or overcorrection (too low velocity, Fig. 8a). Comparison between the migrated CIGs applying the starting (Fig. 8a) and the updated velocity field (Fig. 8b) shows a marked improvement, both in the shallow and deep parts of the seismic data. Below the carbonate reflector, it was not possible to obtain reliable results with this technique due to the overall low signal-to-noise ratio along the line and limited streamer length compared to the larger investigated depth (4,500 m). Therefore, we assigned the velocities to the deeper part of the model on the basis of the sonic log of the Amanda 1bis well. The log shows a velocity inversion in correspondence of the Carnian unconformity, where the velocity decreases from 6,500 (carbonate layers) to 4,600 m/s (terrigenous and volcanic layers), and, then, increases to 6,000 m/s (carbonatic layers) up to the end of the well at about 7,300 m b.s.l. The velocity assigned above the Carnian unconformity is noticeably fairly accurate, as the reflections of the Carnian unconformity show a good flatness on the final CIGs (see the arrows in Fig. 8b). The final velocity model was used to perform a Kirchhoff PSDM of the CROP95-M18 line.

To ensure the accuracy of the velocity model, we carried out travel time tomography of the first arrivals using the CAT3D software (Böhm and OGS research group, 2014). We picked the first arrivals on 360 shot gathers, taking into account the ray paths associated with the diving waves. In this way, only the velocity distribution as a function of depth is updated by the tomography (without defining the horizons). The inversion implemented in the CAT3D software uses an iterative procedure based on the SIRT (Simultaneous Iterative Reconstruction Technique)
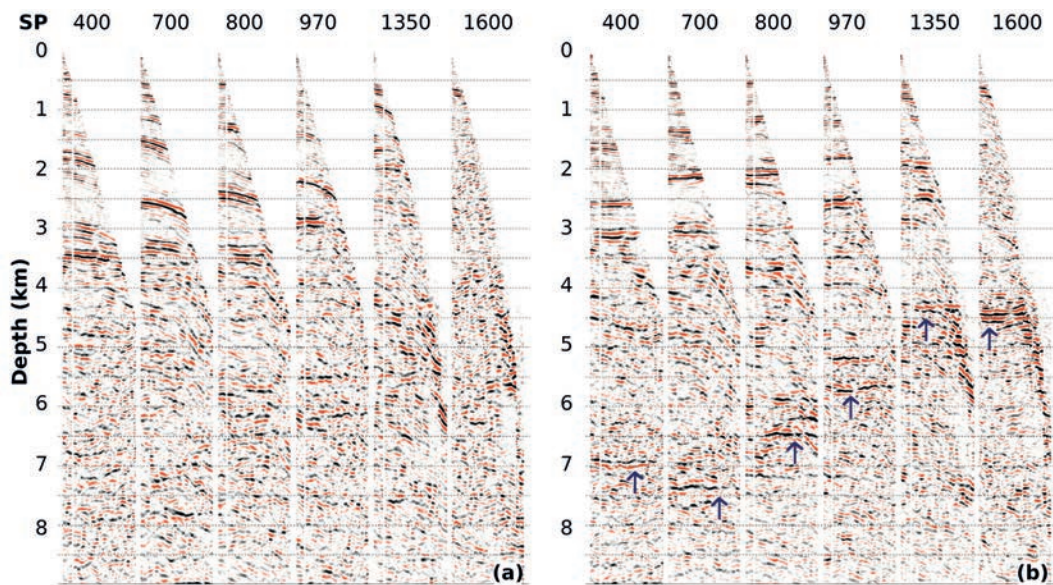
Fig. 8 - Comparison of some representative CIGs migrated with the starting velocity model (a) and the final velocity model updated by the layer-based tomography (b). The arrows show the reflection associated with the Carnian unconformity.

algorithm (Gilbert, 1972). The initial model was created with 100-m wide square cells, while the final model was obtained after 20 tomographic inversion iterations. The reliability of the result achieved was measured by performing a residual analysis (the difference between the observed and calculated travel times), which gave an RMS residual percentage of less than 2%.

4. Results and discussion

The reprocessed PSTM section (Fig. 9) benefits from the great efforts made to increase the signal-to-noise ratio (attenuating coherent and incoherent noise), the temporal and spatial resolution, and the frequency bandwidth. Obviously, on the PSTM section the diffraction hyperbolas have been collapsed and this result cannot be strictly compared to the vintage processed section (since it is only a stacked section).

The energy penetration is very high, with signals detectable even in the deepest part of the section (up to 12-14 s TWT). In general, the vintage section shows more uniform amplitude balancing, which makes the interpretation of these signals more difficult; while in the reprocessed PSTM section (Fig. 9a), the amplitudes of these deep signals stand out more clearly from the background noise. The sub-horizontal reflections at about 8.5 s TWT and 11 s TWT are more visible in the reprocessed section (Fig. 9a) than in the original one (Fig. 9b). These events were interpreted by Finetti and Del Ben (2005) as the top of the lower crust and the Moho, respectively; the latter dipping down to 13 s TWT towards NE. Moving upwards, between 3 s to 6.5 s TWT, from SP 300 to 1,000, below the Carnian unconformity reflector, an area characterised by high amplitude reflectors can now be better identified (Fig. 10a) compared to the vintage stacked section (Fig. 10b), which is highly contaminated by diffraction hyperbolas, thus preventing a satisfactory seismic image. The reflections in this area belong to the Permian - Middle Triassic units, constituted by carbonates, vulcanites and terrigenous sediment, and arranged in a series of
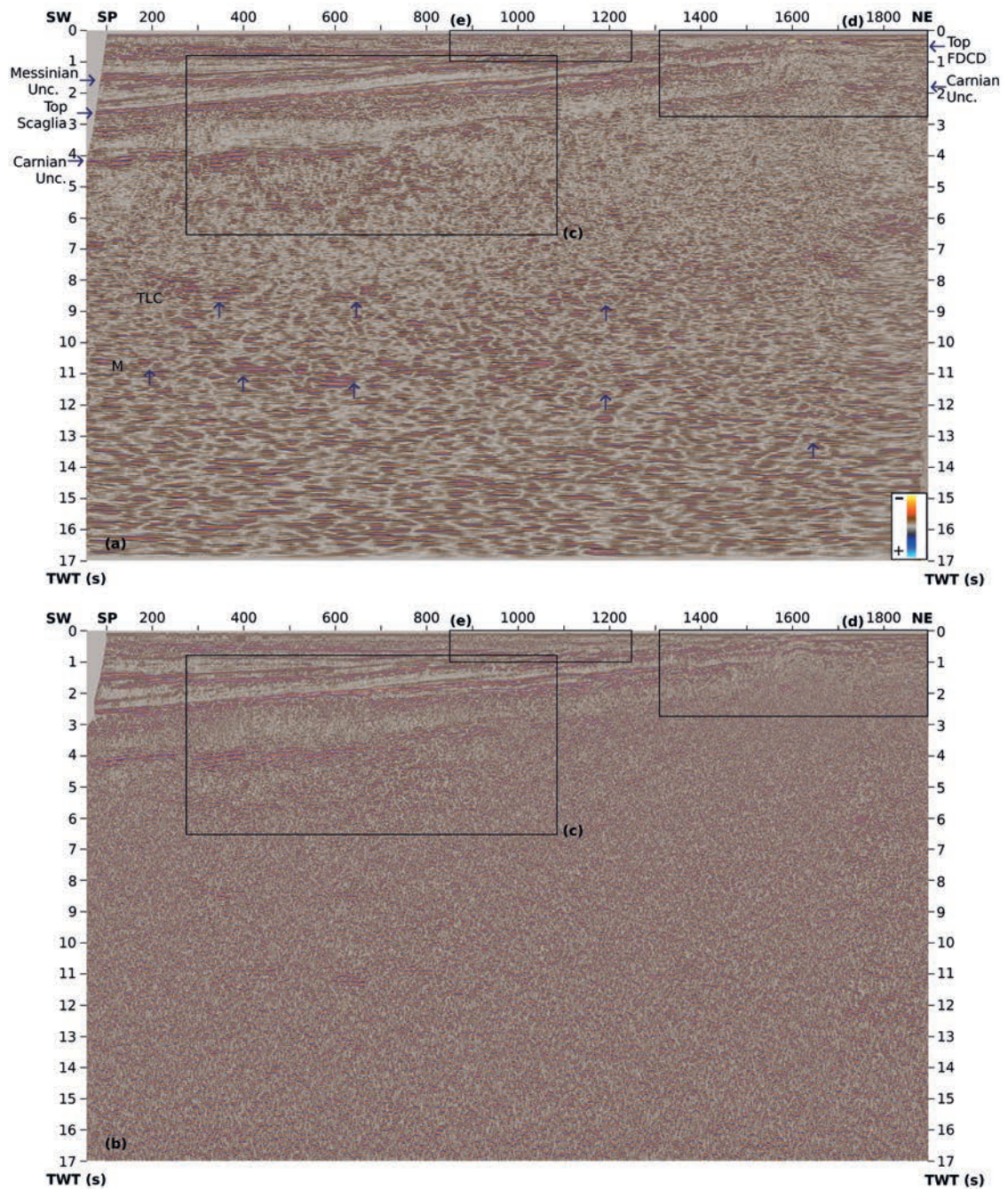
Fig. 9 - The CROP95-M18 section in its PSTM final version (a) and original stacked version (b). The three black rectangles (c), (d) and (e) depict the three areas that are magnified and shown respectively in Figs. 10, 11, and 12. The blue arrows highlight the deep reflectors interpreted by Finetti and Del Ben (2005) respectively as the top lower crust (TLC) and Moho (M).

sub-basins topped by the terrigenous Travenanzes formation. In addition, the PSTM reprocessed profile clearly shows a displacement of approximately 200 ms TWT in the Carnian unconformity due to a normal fault (Fig. 10a).
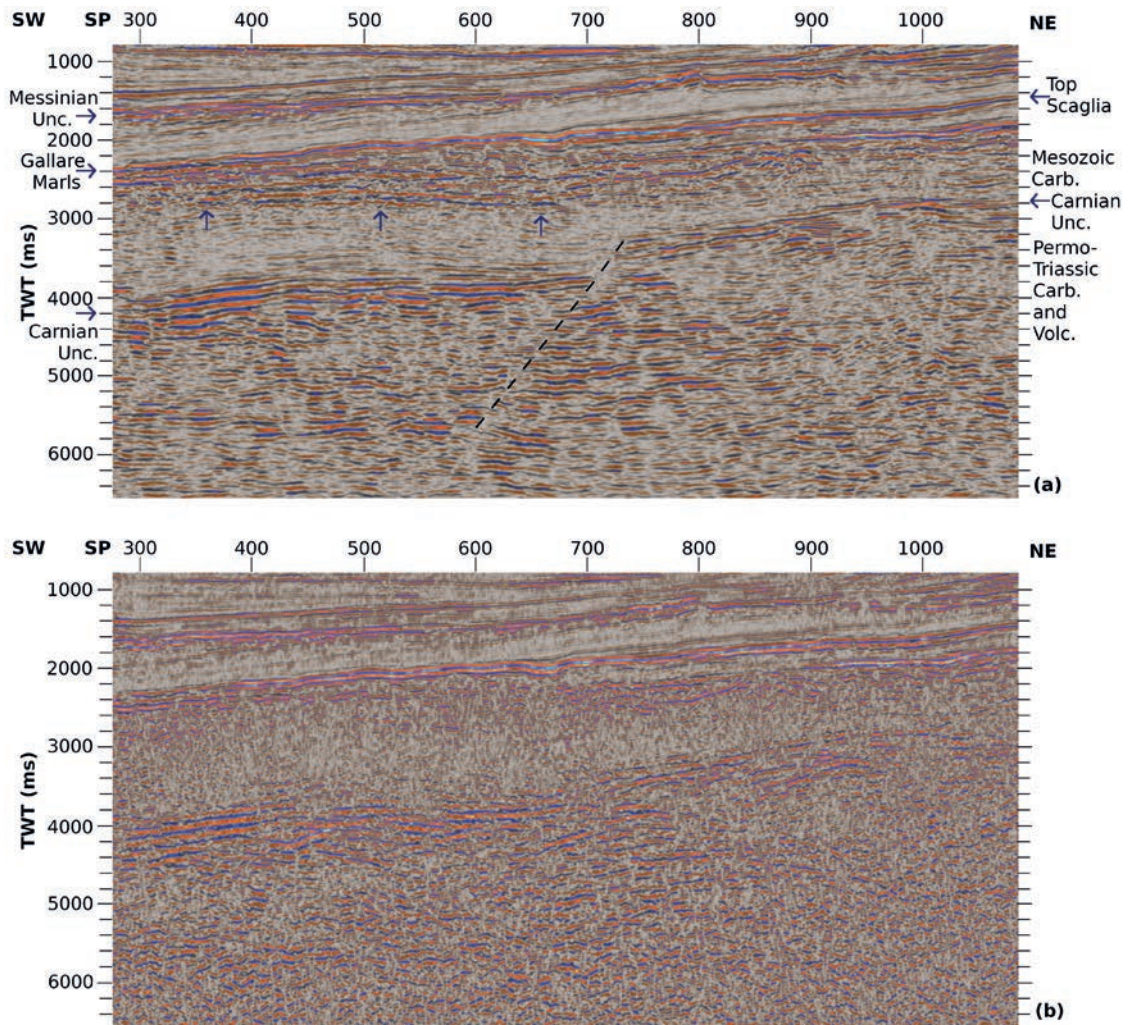
Fig. 10 - Blow-up of a portion of CROP95-M18 section [depicted by the rectangle (e) of Fig. 9], in its PSTM final version (a) and original stacked version (b). The blue arrows highlight the improved image of the reflector at the top of the faint stratified acoustic facies related to the Mesozoic carbonate sequences. The displacement of the Carnian unconformity by normal fault by about 200 ms TWT is clearly imaged.

The images of the eastern part of the section call into question the Dinaric foredeep where a thick sequence of Eocene flysch overlies the FDCP (Busetti *et al.*, 2010). A significant improvement of the reprocessed section (Fig. 11a) compared to the old stacked section (Fig. 11b) is due to the strong attenuation of the multiples, allowing an improvement in the quality of the primary events associated with the top of the flysch and the NE-dipping FDCP (Fig. 11a). Downwards, below the Upper Triassic - Early Cenozoic carbonate units, a reflector can be detected and followed along the entire section, rising from SW towards NE from about 4 s TWT (SP 100, Fig. 9a) to about 1.6 s TWT (SP 1650, Fig. 11a). Thanks to the strategy applied to remove multiples and improve the signal-to-noise ratio, this reflector is now visible also below the Meso-Cenozoic FDCP and represents one of the main results achieved by the reprocessing carried out. This reflector, according to the Amanda 1bis well related to the Carnian unconformity, shows a polarity inversion (due to a velocity inversion also reported by the sonic log and related to the
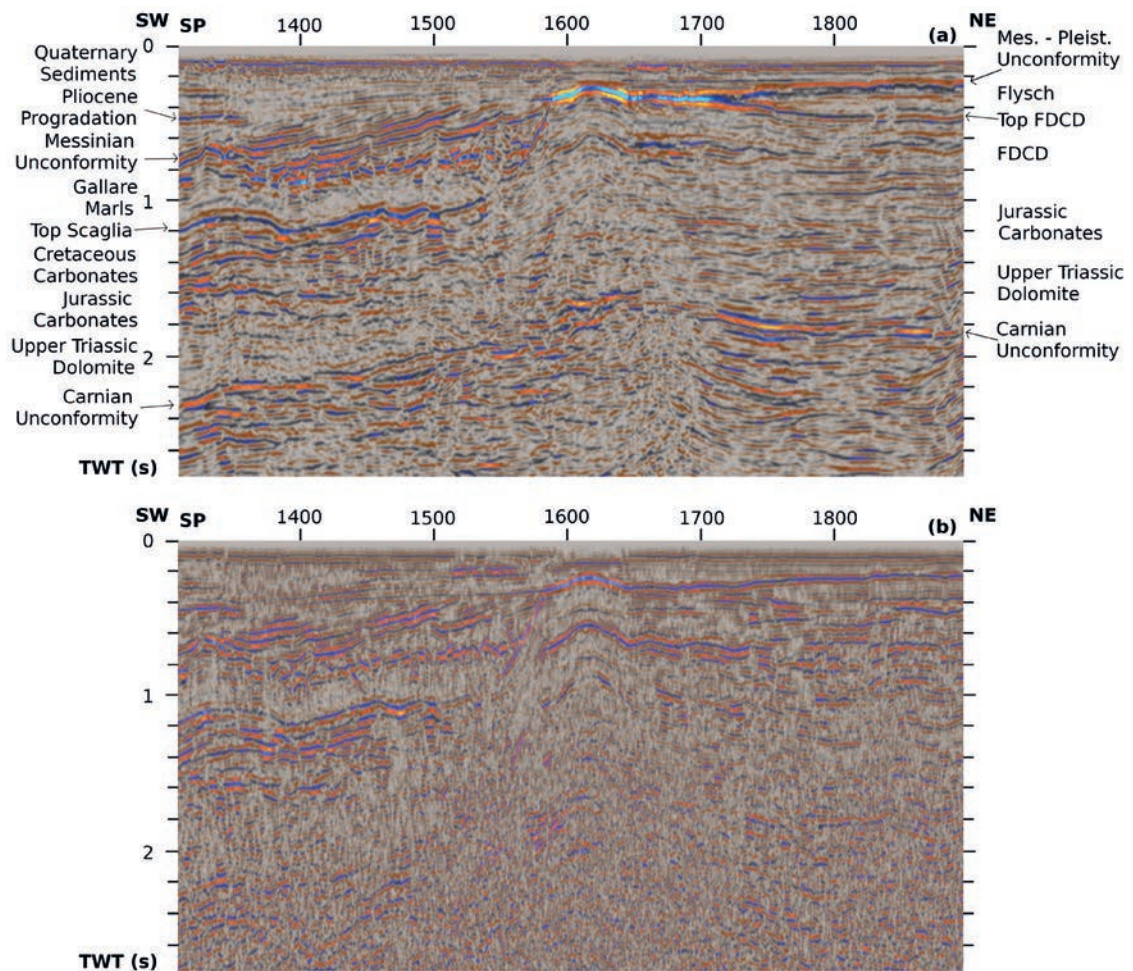
Fig. 11 - Blow-up of a portion of CROP95-M18 section [depicted by the rectangle (d) of Fig. 9], in its PSTM final version (a) and original stacked versions (b). Due to the multiple removal, in the PSTM final version the Carnian unconformity is well imaged.

presence of terrigenous sediment of the Travenanzes formation) and a higher continuity over the whole section. Above the Carnian unconformity, the low amplitude acoustic facies correspond to the Dolomia Principale, an extensive carbonate platform, almost 1,000 m thick, that developed during the Norian in NE Italy.

Moving to the shallow part of the section, it is apparent that the reprocessed data show an improved resolution and a higher continuity of the main reflectors (Fig. 12). The uppermost part shows the Pliocene SW-ward progradation overlain by the NE-ward Pleistocene paleo-Po progradation (Zecchin *et al.*, 2022). Some shallow reflectors of the Quaternary marine and continental sediments (such as the reflector at about 400 ms TWT, at the top of the Pleistocene paleo-Po prograding system) are now evident (or more evident compared to the vintage section) and continuous along the section.

The final velocity model, obtained by combining coherency inversion and layer-based reflection tomography, represents the average interval velocities of the main geological units (Fig. 13). In the central part of the line (around SP 940), the velocity field obtained is consistent with the
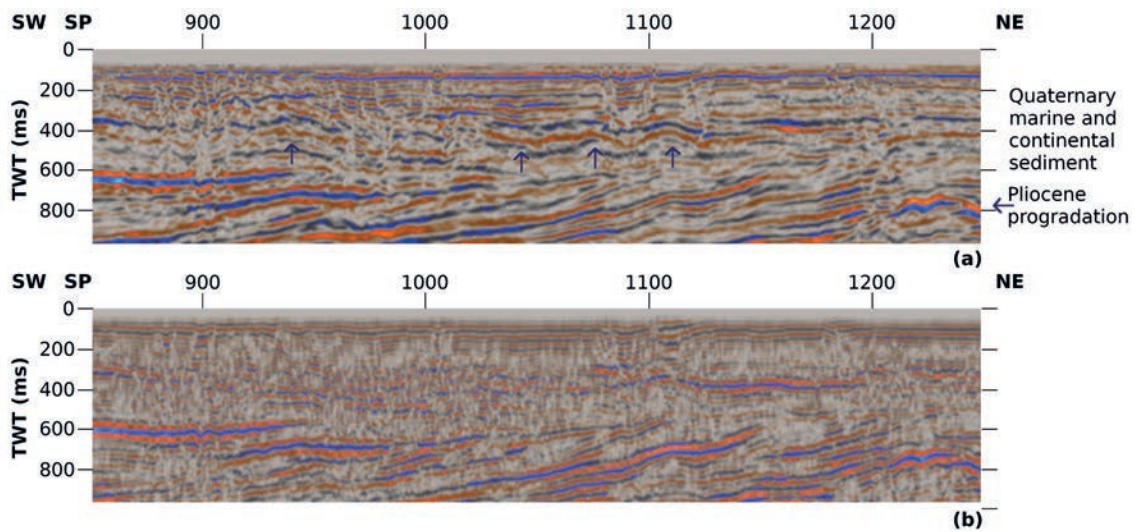
Fig. 12 - Blow-up of a portion of CROP95-M18 section [depicted by the rectangle (c) of Fig. 9], in its PSTM final version (a) and original stacked version (b). The blue arrows highlight the improved image of some reflectors related to the Quaternary paleo-Po northward progradations overlain by the subhorizontal marine and continental Quaternary sediments.

Amanda 1bis sonic log velocities (from Patricelli and Poli, 2020). In particular, the main lithological changes, within the stratigraphic sequence, are marked by clear velocity discontinuities in the model. As a matter of fact, in the shallower part of the Quaternary Asti sands (e.g. first 550 m), the velocity model shows an average velocity of about 1,850 m/s. Thereafter, the velocity increases to 2,250 m/s up to a depth of about 1,100 m b.s.l. (in this depth range, the stratigraphy indicates the presence of Asti sands up to a depth of 800 m b.s.l. and Santerno clays up to
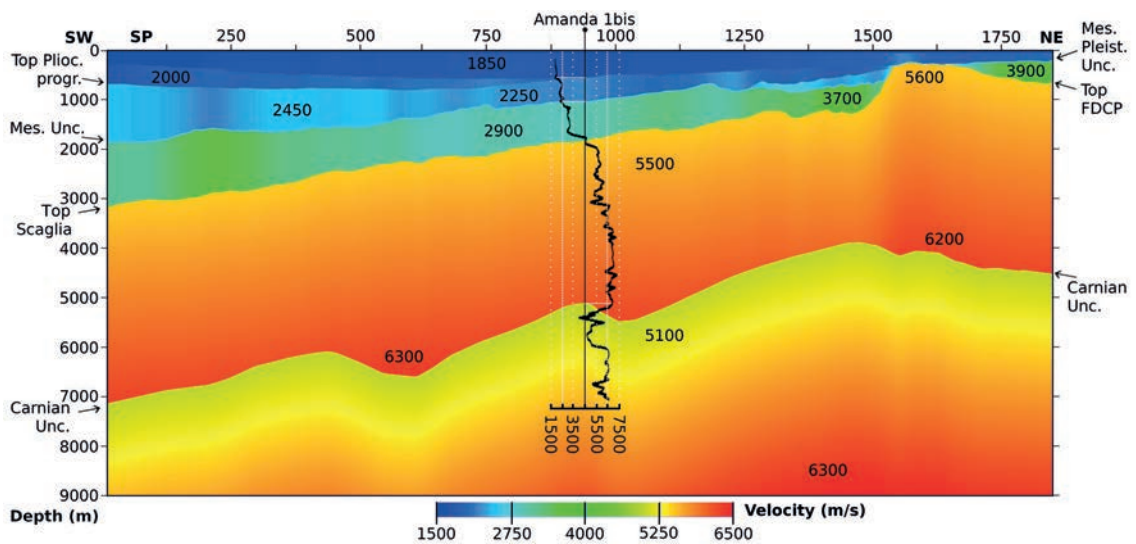

Fig. 13 - The CROP95-M18 velocity model. The sonic log of the Amanda 1bis well is also shown with its velocity scale (modified from Patricelli and Poli, 2020). The velocity discontinuities follow the horizons picked for the coherency inversion technique.

the end of this interval). Between 1,100 m and 1,800 m b.s.l. (where 100 m of Eraclea sands, followed by the Gallare marls, are encountered) the mean velocity is approximately 2,900 m/s. Deeper than 1,800 m, the velocity increases steeply, first in the Scaglia (with a 100-m thickness) and, then, in the Mesozoic carbonates, where the velocity ranges between 5,500 and 6,300 m/s down to a depth of 5,300 m b.s.l.

In the eastern part of the section, starting from SP 1500, the carbonate unit velocity ranges between 5,600 (below the top of the FDCP) and 6,200 m/s (at the level of the Carnian unconformity). Moreover, the flysch unit around SP 1750 has a velocity of about 3,900 m/s, which is consistent with other studies such as Dal Cin (2018), Picotti *et al.* (2018), Accaino *et al.* (2019), Vesnaver *et al.* (2020, 2021), and Dal Cin *et al.* (2022).

In the shallow north-eastern part of the profile (down to a depth of about 1,500 m b.s.l.), further validation was performed using the first-arrival traveltime tomography (diving wave tomography, Fig. 14b). This type of tomography provides a smoother velocity field without significant velocity discontinuities, especially in the presence of weak velocity variations. Therefore, in the south-western and central part of the profile, characterised by a thick and mostly homogeneous terrigenous sediment cover (associated with relatively smaller velocity variations), the comparison with the reflection velocity model (Fig. 14a) is difficult. Nevertheless, the high velocity contrast associated with the contact between the terrigenous sediments of the flysch and the carbonates is well-resolved by the diving wave tomography in the north-eastern area and is in accordance with the velocities obtained with the layer-based tomography (Fig.
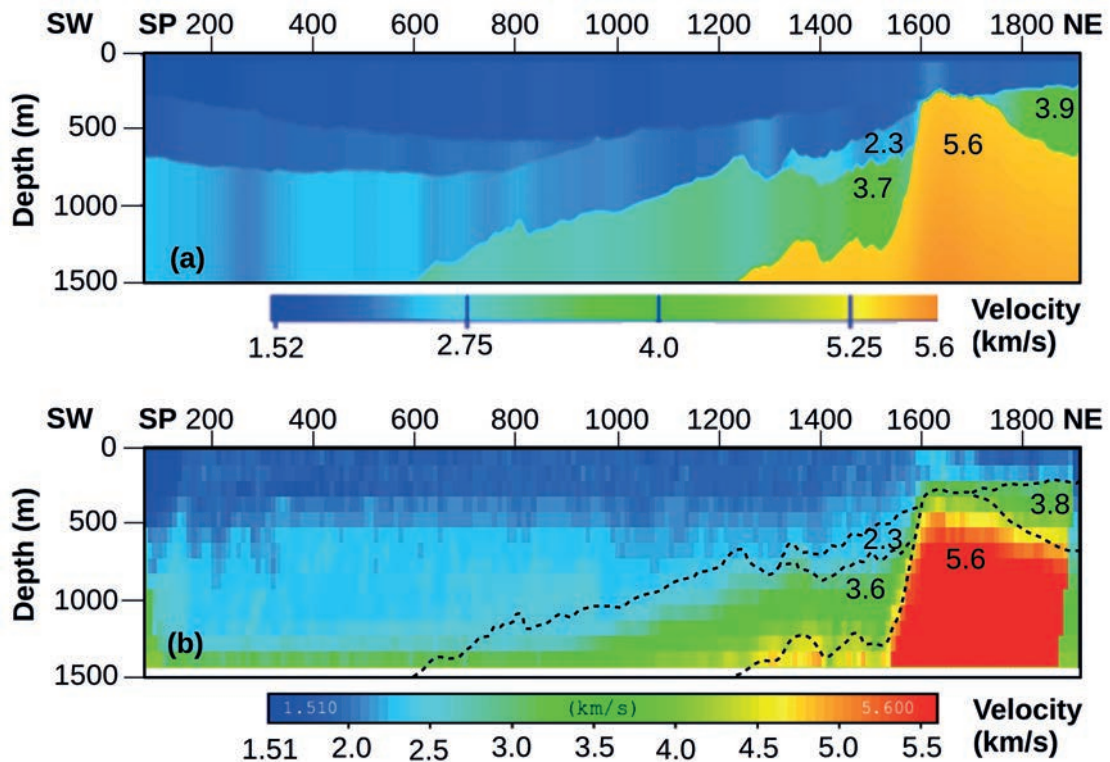

Fig. 14 - Comparison between the velocity model obtained by the reflection tomography (a) and the velocity model obtained by the first arrival traveltime tomography (b). The dashed black lines represent some velocity discontinuities of the reflection tomography velocity model superimposed on the first arrival tomography velocity model.

14a). In particular, the high carbonates, with their steep flanks and high velocity (5,600 m/s), are represented well by both tomographic approaches.

The velocity model obtained after reflection tomography (Fig. 13) was used to perform the Kirchhoff PSDM of the seismic data. The lithostratigraphy of the Amanda 1bis well enabled the validation of the migration result in the central part of the line. There is close consistency between the depths of the main lithostratigraphic units found in the borehole and those indicated by the seismic line (Fig. 15). This is particularly evident at the transition zone between the Pliocene Santerno clays and Quaternary Asti sands, in correspondence of the Messinian unconformity; at the transition between the Gallare marls and the Scaglia (about 1,800 m b.s.l.), the Soccher Limestone and the Marne a Fucoidi formation (about 2,600 m b.s.l.), and at the Carnian unconformity (about 5,300 m b.s.l.). The latter lies at depths varying between 7,500 m (SW) and 4,600 m b.s.l. (NE).
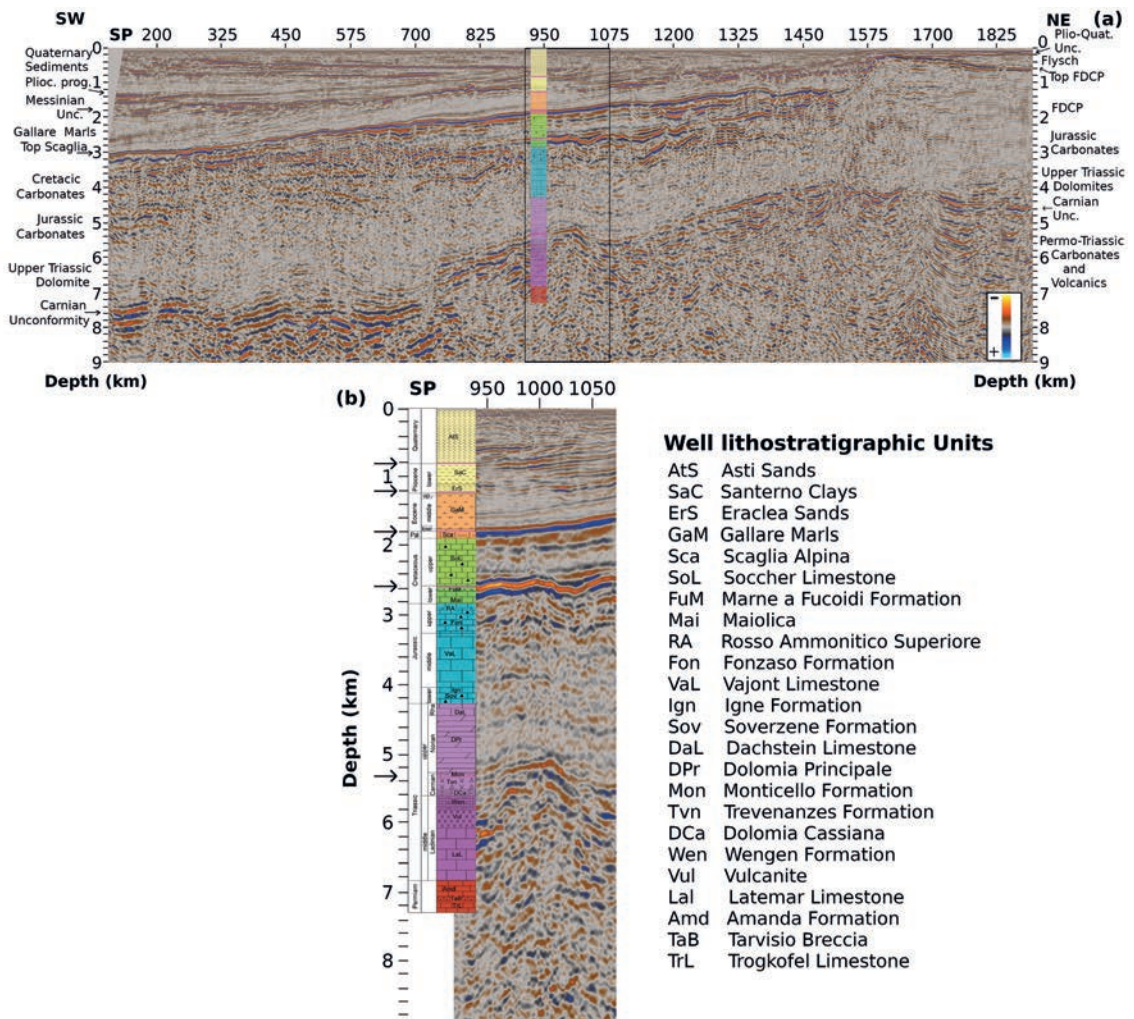

Fig. 15 - The PSDM CROP95-M18 section (a). The black rectangle depicts the area expanded in panel b, where the Amanda 1bis well stratigraphy is superimposed on the section. The arrows indicate the main lithological changes, corresponding to the horizons used for the coherency inversion technique and reflection tomography.

5. Conclusions

We reprocessed the CROP95-M18 seismic line through a modern broadband processing sequence in the time domain. The final PSTM section shows a significant improvement compared to the vintage processed stacked section. In particular, reprocessing enables to increase the signal-to-noise ratio by attenuating coherent and incoherent noise. The multiples attenuation strategy (by combining multichannel predictive tau-*p* deconvolution and SRME) applied proved particularly effective and enhanced the Carnian unconformity reflector that can now be interpreted also below the top of the FDCP. To obtain a reliable interval velocity model down to a depth of 4.5 km, we used the coherency inversion technique followed by a layer-based tomography approach. Velocity information, extracted from the sonic log of the Amanda 1bis well, validated the velocity model in the central part of the CROP95-M18 profile and permitted the assignment of reliable velocities to the deeper part of the model (for depths greater than 4,500 m). Furthermore, the north-eastern part of the velocity model, down to a depth of 1,500 m b.s.l., was validated by the first arrival tomography velocity field. The analysis of the RMOs on the CIGs confirmed the accuracy of the velocity field. In addition, the stratigraphy of the Amanda 1bis well enabled the verification of the main reflector depths in the central part of the line and confirmed the accuracy of the migration results. All the applied methods demonstrated that the value of heritage data can be significantly increased by using the up-to-date processing technology. This is particularly important nowadays, as the collection of new data is difficult, especially for research institutions. The lack of financial resources (due to the energy transition) and limitations (due to environmental impacts), especially for high penetration seismic surveys that require a large amount of released energy, impede the acquisition of new data. For all these reasons, old regional projects, among which the CROP project, are of great importance to the scientific community and need to be constantly updated by reprocessing the data with modern techniques to renew their value.

REFERENCES

Abma R., Kabir N., Matson K.H., Michell S., Shaw S.A. and McLain B.; 2005: *Comparisons of adaptive subtraction methods for multiple attenuation.* The Leading Edge, 24, 277–280, doi: 10.1190/1.1895312.

Accaino F., Busetti M., Böhm G., Baradello L., Affatato A., Dal Cin M. and Nieto D.; 2019: *Geophysical investigation of the Isonzo Plain (NE Italy): imaging of the Dinaric-Alpine chain convergence zone*. Ital. J. Geosci., 138, 202-215, doi: 10.3301/IJG.2019.01.

Ambrosetti P., Bosi F., Carraro F., Ciaranfi N., Panizza M., Papani G., Vezzani L. and Zanferrari A.; 1987: *Neotectonic map of Italy, scale 1:500.000*. Consiglio Nazionale delle Ricerche, Roma, Italy.

Arso; 2017: *Slovenian Environment Agency.* Ministry of the Environment and Spatial Planning, Ljubljana, Slovenia. <https://gis.arso.gov.si>.

Berra F., Stucchi E.M. and Moretti S.; 2019: *New information from "old" seismic lines: an updated geological interpretation from the re-processing of the CROP line M-2A/I (Bonifacio Straits) at shallow depths.* Ital. J. Geosci., 138, 31-42, doi: 10.3301/IJG.2018.24.

Böhm G. and OGS research group; 2014: *Cat3D. Computer Aided Tomography for 3-D models, User manual.* Istituto Nazionale di Oceanografia e Geofisica Applicata (OGS), Trieste, Italy, 60 pp.

Boiero D., Wiarda E. and Vermeer P.; 2013: *Surface- and guided-wave inversion for near-surface modeling in land and shallow marine seismic data*. The Leading Edge, 32, 638-646, doi: 10.1190/tle32060638.1.

Brancatelli G., Forlin E., Bertone N., Del Ben A. and Geletti R.; 2022: *Chapter 7 - Time to depth seismic reprocessing of vintage data: a case study in the Otranto Channel (south Adriatic Sea)*. In: Bell R., Iacopini D. and Vardy M. (eds), Interpreting Subsurface Seismic Data, Elsevier, Amsterdam, The Netherlands, pp. 157-197, doi: 10.1016/B978-0-12-818562-9.00009-1.

Burg K.E., Ewing M., Press F. and Stulken E.J.; 1951: *A seismic wave guide phenomenon.* Geophysics, 16, 594–612, doi:10.1190/1.1437708.

Burrato P., Poli M.E., Vannoli P., Zanferrari A., Basili R. and Galadini F.; 2008: *Sources of Mw 5+ earthquakes in northeastern Italy and western Slovenia: an updated view based on geological and seismological evidence.* Tectonophys., 453, 157-176, doi: 10.1016/j.tecto.2007.07.009.

Busanello G., Del Ben A. and Pipan M.; 2017: *Petroleum systems modelling as an exploration tool: from surface seismic acquisition to basin modelling: a case study from a periplatform basin in northern Adriatic.* First Break, 35, 69-76, doi: 10.3997/1365-2397.35.3.87564.

Busetti M., Volpi V., Nicolich R., Barison E., Romeo R., Baradello L., Brancatelli G., Giustiniani M., Marchi M., Zanolla C., Nieto D., Ramella R. and Wardell N.; 2010: *Dinaric tectonic features in the Gulf of Trieste (northern Adriatic)*. Boll. Geof. Teor. Appl., 51, 117-128.

Cati A., Sartorio D. and Venturini S.; 1987: *Carbonate platforms in the subsurface of the northern Adriatic area*. Mem. Soc. Geol. Ital., 40, 295-308.

Civile D., Brancolini G., Lodolo E., Forlin E., Accaino F., Zecchin M. and Brancatelli G.; 2021: *Morphostructural setting and tectonic evolution of the central part of the Sicilian Channel (central Mediterranean)*. Lithos., 2021, 7866771, 24 pp., doi: 10.2113/2021/7866771.

Cucchi F., Piano C., Fanucci F., Pugliese N., Tunis G. and Zini L.; 2013: *Brevi note illustrative della carta geologica del Carso Classico italiano*. Servizio Geologico, Direzione Centrale Ambiente Energia e Politiche per la Montagna, Regione Autonoma Friuli Venezia Giulia, Trieste, Italy, Progetto GEO-CGT, Cartografia Geologica di sintesi in scala 1:10.000, 43 pp.

Dal Cin M.; 2018: *3D velocity depth model in the Gulf of Trieste by means of tomographic analysis from multichannel seismic reflection data*. Ph.D. Thesis in Earth Science and Fluid Mechanics, XXX cycle, University of Trieste, OGS and ICTP, Trieste, Italy, 212 pp. <hdl.handle.net/11368/2922569>.

Dal Cin M., Böhm G., Busetti M., Picotti S., Zgur F. and Camerlenghi A.; 2022: *3D velocity-depth model from multichannel seismic in the Dinaric foredeep of the Gulf of Trieste (Adriatic Sea), at the NE edge of Adria plate*. Tectonophys., 838, 229470, 16 pp., doi: 10.1016/j.tecto.2022.229470.

Dondurur D.; 2018: *Acquisition and processing of marine seismic data*. Elsevier, Amsterdam, The Netherlands, 598 pp., doi: 10.1016/C2016-0-01591-7.

EEA (European Environment Agency); 2017: *Copernicus land monitoring service EU-DEM*. European Union, Brussels, Belgium. <www.eea.europa.eu/data-and-maps/data/copernicus-land-monitoring-service-eu-dem>.

EMODnet Bathymetry Consortium; 2018: *EMODnet digital bathymetry*. European Marine Observation and Data Network, European Commission, Brussels, Belgium. <www.emodnet.eu>.

Fantoni R., Catellani D., Merlini S., Rogledi S. and Venturini S.; 2002: *La registrazione degli eventi deformativi cenozoici nell'avampaese veneto-friulano*. Mem. Soc. Geol. Ital., 57, 301-313.

Finetti I.R (ed); 2005: *CROP PROJECT: Deep seismic exploration of the central Mediterranean and Italy.* Atlases Geoscience 1, Elsevier, Amsterdam, The Netherlands, 872 pp., ISBN: 9780080457604.

Finetti I.R. and Del Ben A.; 2005: *Crustal tectono-stratigraphic setting of the Adriatic Sea from new CROP seismic data*. In: Finetti I.R. (ed), CROP PROJECT: Deep Seismic Exploration of the Central Mediterranean and Italy, Elsevier, Amsterdam, The Netherlands, pp. 519-547.

Finetti I.R., Forlin E. and Pipan M.; 2005: *CROP seismic data acquisition, processing and interpretative reprocessing*. In: Finetti I.R. (ed), CROP PROJECT: Deep Seismic Exploration of the Central Mediterranean and Italy, Elsevier, Amsterdam, The Netherlands, pp. 81-101.

Galadini F., Poli M.E. and Zanferrari A.; 2005: *Seismogenic sources potentially responsible for earthquakes with M ≥ 6 in the eastern Southern Alps (Thiene-Udine sector, NE Italy)*. Geophys. J. Int., 161, 739-762, doi: 10.1111/j.1365-246X.2005.02571.x.

Gilbert P.F.C; 1972: *An iterative method for three-dimensional reconstruction of an object from projections*. J. Theor. Biol., 36, 105-117.

Giustiniani M., Tinivella U., Parolai S., Donda F., Brancolini G. and Volpi V.; 2020: *Integrated geophysical analyses of shallow-water seismic imaging with Scholte wave inversion: the northern Adriatic Sea case study*. Front. Earth Sci., 8, 587898, 9 pp., doi: 10.3389/feart.2020.587898.

Giustiniani M., Busetti M., Dal Cin M., Barison E., Cimolino A., Brancatelli G. and Baradello L.; 2022: *Geophysical and geological views of potential water resources in the north-eastern Adriatic Sea.* Geosci., 12, 139, 14 pp., doi: 10.3390/geosciences12030139.

Henley D.C.; 1999: *The radial trace transform: an effective domain for coherent noise attenuation and wavefield separation*. In: SEG Technical Program Expanded Abstracts 1999, Society of Exploration Geophysicists, Tulsa, OK, USA, pp. 1204-1207, doi: 10.1190/1.1820721.

Hung B., Yang K., Zhou J., Guo Y. and Long Xia Q.; 2010: *Surface multiple attenuation in seabeach-shallow water, case study on data from the Bohai Sea*. In: SEG Technical Program Expanded Abstracts 2010, Society of Exploration Geophysicists, Tulsa, OK, USA, pp. 3431-3435, doi: 10.1190/1.3513561.

IDT-RV; 2017: *Infrastruttura Dati Territoriali.* Regione del Veneto, Ambiente e Territorio, Venezia, Italy. <idt2.regione.veneto.it>.

IRDAT-FVG; 2017: *L'Infrastruttura Regionale dei Dati Ambientali e Territoriali.* Regione Autonoma Friuli Venezia Giulia, Conoscere l'ambiente e il territorio, Trieste, Italy. <irdat.regione.fvg.it/WebGIS/>.

Jones I.F.; 2010: *Tutorial: ray-based tomography.* First Break, 28, 45-52, doi: 10.3997/1365-2397.2010006.

Jones I.F.; 2018: *Velocities, imaging and waveform inversion*. EAGE publications, 238 pp., ISBN: 978-94-6282-253-5, doi: 10.3997/book9789462822535.

Jurkovšek B., Biolchi S., Furlani S., Kolar-Jurkovšek T., Zini L., Jež J., Tunis G., Bavec M. and Cucchi F.; 2016: *Geology of the Classical Karst Region (SW Slovenia - NE Italy)*. J. Maps, 12, 352-362, doi: 10.1080/17445647.2016.1215941.

Kugler S., Bohlen T., Forbriger T., Bussat S. and Klein G.; 2007: *Scholte-wave tomography for shallow-water marine sediments*. Geophys. J. Int., 168, 551-570, doi: 10.1111/j.1365-246X.2006.03233.x.

Landa E., Kosloff D., Keydar S., Koren Z. and Reshef M.; 1988: *Method for determination of velocity and depth from seismic reflection data*. Geophys. Prospect., 36, 223-243, doi: 10.1111/j.1365-2478.1988.tb02161.x.

Liner C.L.; 2012: *Elements of seismic dispersion: a somewhat practical guide to frequency-dependent phenomena.* Society of Exploration Geophysicists, Tulsa, OK, USA, Series 15, 193 pp., doi: 10.1190/1.9781560802952.

Lokshtanov D.; 1995: *Multiple suppression by single channel and multichannel deconvolution in the tau-p domain*. In: SEG Technical Program Expanded Abstracts 1995, Society of Exploration Geophysicists, Tulsa, OK, USA, pp. 1482-1485, doi: 10.1190/1.1887243.

Lokshtanov D.; 1999: *Multiple suppression by data–consistent deconvolution.* The Leading Edge, 18, 115-119, doi: 10.1190/1.1438136.

Mazzotti A., Stucchi E., Fradelizio G.L., Zanzi L. and Scandone P.; 2000: *Seismic exploration in complex terrains: a processing experience in the Southern Apennines.* Geophys., 65, 1402-1417, doi: 10.1190/1.1444830.

Munteanu I., Diviacco P., Sauli C., Dinu C., Burcă M., Panin N. and Brancatelli G.; 2018: *New insights into the Black Sea basin in the light of the reprocessing of vintage regional seismic data*. In: Finkl C. and Makowski C. (eds), Diversity in Coastal Marine Sciences, Coastal Research Library, Springer International Publishing, Cham, Switzerland, vol. 23, pp. 91-114, doi: 10.1007/978-3-319-57577-3_6.

Nicholls H., Penn L., Marszalek A., Esestime P., Rodriguez K., Benson C. and Cvetkovic M.; 2015: *The role of legacy seismic in exploring new offshore hydrocarbon provinces - or can you "teach" old data new tricks (technologies)?*. In: SEG Technical Program Expanded Abstracts 2015, Society of Exploration Geophysicists, Tulsa, OK, USA, pp. 1917-1921, doi: 10.1190/segam2015-5875295.1.

Nicolich R., Della Vedova B., Giustiniani M. and Fantoni R.; 2004: *Carta del sottosuolo della Pianura Friulana*. Regione Autonoma Friuli Venezia Giulia, Direzione Centrale Ambiente e Lavori Pubblici, Servizio Geologico, Trieste, Italy, 32 pp.

Oppenheim A.V. and Schafer R.W.; 1989: *Discrete-Time signal processing, 1st ed.* Prentice Hall, Englewood Cliffs, NJ, USA, 879 pp.

Patricelli G. and Poli M.E; 2020: *Quaternary tectonic activity in the north-eastern Friuli Plain (NE Italy)*. Boll. Geof. Teor. Appl., 61, 309-332, doi: 10.4430/bgta0319.

Peacock K.L. and Treitel S.; 1969: *Predictive deconvolution: theory and practice.* Geophys., 34, 155-169, doi: 10.1190/1.1440003.

Perz M.J. and Masoomzadeh H.; 2014: *Deterministic marine deghosting: tutorial and recent advances.* In: Expanded Abstracts, FOCUS GeoConvention, Calgary, AB, Canada, 90224, 6 pp.

Picotti S., Dal Cin M., Böhm G. and Busetti M.; 2018: *Evidences of seismic Flysch anisotropy in the Gulf of Trieste*. In: Proc. 24th European Meeting of Environmental and Engineering Geophysics, European Association of Geoscientists & Engineers, Porto, Portugal, pp. 1-5, doi: 10.3997/2214-4609.201802637.

Placer L., Vrabec M. and Celarc B.; 2010: *The bases for understanding of the NW Dinarides and Istria Peninsula tectonics*. Geologija, 53, 55-86, doi: 10.5474/geologija.2010.005.

Rauch D.; 1986: *On the role of bottom interface waves in ocean seismo-acoustics: a review.* In: Akal T. and Berkson J.M. (eds), Ocean Seismo-Acoustics, Plenum, London, UK, pp. 623-641, doi: 10.1007/978-1-4613-2201-6_60.

Robinson E.A. and Treitel S.; 1980: *Geophysical signal analysis*. Prentice Hall, Englewood Cliffs, NJ, USA, 466 pp.

Scholte J.G.; 1942: *On the Stoneley wave equation*. In: Proc. Koninklijke Nederlandse Akademie van Wetenschappen, 45, part 1, pp. 20-25.

Scholte J.G.; 1947: *The range of existence of Rayleigh and Stoneley waves*. Geophysical Supplements to the Monthly Notices of the Royal Astronomical Society, 5, 120-126, doi: 10.1111/j.1365-246X.1947.tb00347.x.

Scrocca D., Doglioni C., Innocenti F., Manetti P., Mazzotti A., Bertelli L. and D'Offizi S. (eds); 2003: *Atlante CROP-Profili sismici a riflessione della crosta italiana*. Memorie descrittive della Carta Geologica d'Italia, 62, 194.

Sopher D. and Juhlin C.; 2013: *Processing and interpretation of vintage 2D marine seismic data from the outer Hanö Bay area, Baltic Sea.* Journal of Applied Geophysics, 95, 1-15, doi: 10.1016/j.jappgeo.2013.04.011.

Taner M.T.; 1980: *Long-period sea-floor multiples and their suppression.* Geophys. Prospect., 28, 30-48, doi: 10.1111/j.1365-2478.1980.tb01209.x.

Taner M.T., O'Doherty R.F. and Koehler F.; 1995: *Long period multiple suppression by predictive deconvolution in the x-t domain*. Geophys. Prospect., 43, 433-468, doi: 10.1111/j.1365-2478.1995.tb00261.x.

Tognarelli A., Stucchi E.M., Musumeci G., Mazzarini F. and Sani F.; 2011: *Reprocessing of the Crop M12A seismic line focused on shallow-depth geological structures in the northern Tyrrhenian Sea*. Boll. Geof. Teor. Appl., 52, 23-38.

Treitel S., Gutowski P.R. and Wagner D.E.; 1982: *Plane-wave decomposition of seismograms.* Geophys., 47, 1375-1401, doi: 10.1190/1.1441287.

Trobec A., Busetti M., Zgur F., Baradello L., Babich A., Cova A., Gordini E., Romeo R., Tomini I., Poglajen S., Diviacco P. and Vrabec M.; 2018: *Thickness of marine Holocene sediment in the Gulf of Trieste (northern Adriatic Sea)*. Earth Syst. Sci. Data, 10, 1077-1092, doi: 10.1016/j.geomorph.2017.03.012.

Verschuur D.J.; 2013: *Seismic multiple removal techniques: past, present and future. Revised Edition.* EAGE publications, 212 pp., ISBN:978-90-73834-56-9.

Verschuur D.J., Berkhout A.J. and Wapenaar C.P.A.; 1992: *Adaptive surface-related multiple elimination.* Geophysics, 57, 1166-1177, doi: 10.1190/1.1443330.

Vesnaver A., Böhm G., Cance P., Dal Cin M. and Gei D.; 2020: *Windowless Q-factor tomography by the instantaneous frequency.* Geophysical Prospecting, 68, 2611–2636, doi: 10.1111/1365-2478.13020.

Vesnaver A., Böhm G., Busetti M., Dal Cin M. and Zgur F.; 2021: *Broadband Q-factor imaging for geofluid detection in the Gulf of Trieste (northern Adriatic Sea)*. Front. Earth Sci., 9, 640194, 16 pp., doi: 10.3389/feart.2021.640194.

ViDEPI Project; 2009: *Visibility of petroleum exploration data in Italy*. Ministry for Economic Development DGRME - Italian Geological Society - Assomineraria, Roma, Italy. <www.videpi.com>.

Wang J., Stewart R.R., Dyaur N.I. and Bell M.L.; 2016: *Marine guided waves: subbottom property estimation and filtering using physical modeling data*. Geophys., 81, V303-V315, doi: 10.1190/geo2015-0401.1.

Yilmaz O.; 2001: *Seismic data analysis.* Society of Exploration Geophysicists, 2065 pp., ISBN 978-1-56080-094-1, doi: 10.1190/1.9781560801580.

Yilmaz O. and Baysal E.; 2015: *An effective ghost removal method for marine broadband seismic data processing.* In: Conference Proceedings, 77th EAGE Conference and Exhibition 2015, Jun 2015, Vol. 2015, pp. 1–5, doi: 10.3997/2214-4609.201413195.

Zampa L.S.; 2020: *New bathymetric maps of the North East Adriatic Sea*. Busetti M. and Camerlenghi A. (eds), National Institute of Oceanography and Applied Geophysics-OGS, Trieste, Italy, Technical Report 05/2020OGS.

Zanferrari A., Avigliano R., Monegato G., Paiero G., Poli M.E., Barbieri S., Calderoni G., Carraro F., Donegana M., Grandesso P., Michelutti G., Pavšic J., Pini R., Ravazzi C., Rogledi S., Stefani C., Tunis G., Wick L. and Zanolla S. (a cura di); 2008: *Note illustrative della Carta Geologica d'Italia alla scala 1: 50.000, foglio 066 Udine*. Agenzia per la Protezione dell'Ambiente e per i Servizi Tecnici (APAT) - Servizio Geologico d'Italia, Regione Autonoma Friuli Venezia Giulia, Servizio Geologico, 176 pp., doi: 10.13140/RG.2.1.3361.2886.

Zanferrari A., Masetti D., Monegato G., Poli M.E., Avigliano R., Carraro F., Faranda C., Grandesso P., Ligios S., Podda F., Ponton M., Rigo R., Roghi G., Romano R., Russo S. and Stefani C.; 2013: *Note illustrative della Carta geologica d'Italia alla scala 1:50.000, foglio 049 Gemona del Friuli*. Servizio Geologico d'Italia - ISPRA, Regione Autonoma Friuli Venezia Giulia, Servizio Geologico, 262 pp.

Zecchin M., Busetti M., Brancatelli G., Dal Cin M. and Zgur F.; 2022: *Plio-Quaternary sequences and tectonic events in the north-eastern Adriatic Sea (northern Italy)*. Mar. Pet. Geol., 142, 105745, 15 pp., doi: 10.1016/j.marpetgeo.2022.105745.

Corresponding author: Giuseppe Brancatelli
                            Istituto di Oceanografia e di Geofisica Sperimentale - OGS
                            Borgo Grotta Gigante 42c, 34016 Sgonico (TS), Italy
                            Phone: +39 040 2140235; e-mail: gbrancatelli@ogs.it